water

MDPI

Article

Soil Erosion under Future Climate Change Scenarios in a Semi-Arid Region

Abdenbi Elaloui [1,*], El Mahdi El Khalki [2], Mustapha Namous [1], Khalid Ziadi [1], Hasna Eloudi [1], Elhousna Faouzi [1], Latifa Bou-Imajjane [3], Morad Karroum [1], Yves Tramblay [4], Abdelghani Boudhar [1,2] and Abdelghani Chehbouni [2]

[1] Data Science for Sustainable Earth Laboratory (Data4Earth), Sultan Moulay Slimane University, Beni Mellal 23000, Morocco
[2] International Water Research Institute, Mohammed VI Polytechnic University, Ben Guerir 43150, Morocco
[3] Geology Department, Faculty of Science Agadir, Ibn Zohr University, Agadir 80000, Morocco
[4] HydroSciences Montpellier, University Montpellier, CNRS, IRD, 34090 Montpellier, France
* Correspondence: a.elaloui@usms.ma; Tel.: +212-(6)-61863358

Abstract: The Mediterranean Region is presumed to be one of the locations where climate change will have the most effect. This impacts natural resources and increases the extent and severity of natural disasters, in general, and soil water erosion in particular. The focus of this research was to assess how climate change might affect the rate of soil erosion in a watershed in the High Atlas of Morocco. For this purpose, high-resolution precipitation and temperature data (12.5 × 12.5 km) were collected from EURO-CORDEX regional climate model (RCM) simulations for the baseline period, 1976–2005, and future periods, 2030–2060 and 2061–2090. In addition, three maps were created for slopes, land cover, and geology, while the observed erosion process in the catchment was determined following field observations. The erosion potential model (EPM) was then used to assess the impacts of precipitation and temperature variations on the soil erosion rate. Until the end of the 21st century, the results showed a decrease in annual precipitation of −32% and −46% under RCP 4.5 for the periods 2030–2060 and 2061–2090, respectively, −28% and −56% under RCP 8.5 for the same periods, respectively, and a large increase in temperature of +2.8 °C and +4.1 °C for the RCP 4.5 scenario, and +3.1 °C and +5.2 °C for the RCP 8.5 scenario for the periods 2030–2060 and 2061–2090, respectively. The aforementioned changes are anticipated to significantly increase the soil erosion potential rate, by +97.11 m^3/km^2/year by 2060, and +76.06 m^3/km^2/year by 2090, under the RCP 4.5 scenario. The RCP 8.5 predicts a rise of +124.64 m^3/km^2/year for the period 2030–2060, but a drop of −123.82 m^3/km^2/year for the period 2060–2090.

Keywords: soil erosion rates; climate change; RCP 4.5; RCP 8.5; EPM model; High Atlas; Morocco

Citation: Elaloui, A.; Khalki, E.M.E.; Namous, M.; Ziadi, K.; Eloudi, H.; Faouzi, E.; Bou-Imajjane, L.; Karroum, M.; Tramblay, Y.; Boudhar, A.; et al. Soil Erosion under Future Climate Change Scenarios in a Semi-Arid Region. *Water* **2023**, *15*, 146. https://doi.org/10.3390/w15010146

Academic Editors: Xudong Peng, Lunjiang Wang and Adimalla Narsimha

Received: 11 December 2022
Revised: 22 December 2022
Accepted: 24 December 2022
Published: 30 December 2022

1. Introduction

Water erosion is among the leading global causes of soil degradation worldwide, and it is considered as one of the major threats to the environment, agriculture, and food security. In addition, numerous recent studies have raised concerns about the dangers of erosion on the world's soil, water, and ecosystems [1,2]. Therefore, soil is considered as a limited natural resource that must be protected [3]. Natural variables, such as rainfall intensity, soil qualities, terrain, vegetation, morphology, drainage network features, and land-use activities, as well as human endeavors, influence the rate of soil erosion [4].

On the global timescale, the climate has an essential moderating impact on erosion and mass loss mechanisms, structuring watersheds and stream systems, and dictating debris output [5]. Moreover, many current soil erosion concerns will exacerbate as a consequence of global change. In this context, desertification may be a result of climate change and rapidly rising human pressures, both of which undermine the long-term viability of soil. Variations in global temperature and precipitation patterns will influence

soil loss in a variety of ways, including changes in rainfall erosivity [6,7]. Soil erosion is expected to be negatively impacted by climate change due to a range of factors, such as the intensity and quantity of precipitation, and the temperature effects on the soil's relative humidity, and vegetation development [8–14]. This is especially perceptible in the hilly regions and southern Mediterranean areas [15]. There, Northwest Africa is extremely sensitive to climate change because of its sensitivity to changes in temperature, freshwater supply, and population [16]. In this context, Morocco is distinguished as one of the most climate-vulnerable countries [15,17–19], especially since around 0.5 percent of the entire water-holding capacity of Moroccan dams is lost annually [20].

To evaluate the siltation of dams and sediment transfer from river basins, managers must estimate the risk of soil erosion and forecast potential future scenarios. To achieve this, numerous methods, techniques, and innovative approaches have been initiated and developed by specialists throughout the globe. Indeed, in the literature, researchers have developed various physical and empirical models for the qualitative and quantitative estimation of soil erosion at the watershed scale. These models range in complexity from simple to complicated, and they vary considerably in their data sets and capacity to forecast soil loss [21]. More recently, using high-resolution satellite imagery, researchers investigated the effect of global warming on soil degradation. In hilly Mediterranean catchments, regional climate models (RCMs) are constrained [22], but no research of this type has been conducted in Morocco, according to the latest findings.

This study aims to assess the impact of climate change on soil degradation in a mountainous Moroccan watershed using the erosion potential model (EPM) and climate simulation of the EURO-CORDEX regional climate model. To do this, we will quantify the soil loss during the reference period 1976–2005, then project future predictions of temperature and precipitation to estimate the loss in two periods, 2030–2060 and 2061–2090, under two climate scenarios, optimistic RCP4.5, and pessimistic RCP8.5. These results will be an important database for effective, sustainable land-use planning that safeguards natural resources.

2. Materials and Methods

2.1. Study Area

The Oum Er-Rbia Great Basin includes the Tassaoute basin, which is upstream of the Moulay Youssef Dam (Figure 1). The Oum Er-Rbia watershed is situated in the middle of Morocco between latitudes 31°15′ N and 33°22′ N and longitudes 5°00′ W and 9°20′ W. It is one of the biggest basins in Morocco, taking up roughly 35,000 km^2 (or 7% of the country's overall size) with a 550 km extension. It is surrounded on its eastern side by the Atlas Mountains, which provide the majority of the water supply for the plains below and contain the longest permanent river, the Oum Er-Rbia (nearly 600 km). Azemmour, which is about 16 km from El Jadida, is where it empties into the Atlantic Ocean after rising to a height of 1800 m in the Middle Atlas, through the Atlas Mountain range, the Tadla plain, and the coastal Meseta.

Our research focuses on the catchment upstream of the Moulay Youssef Dam, which is a part of the northern region of the sub-Atlasic of the Demnate High Atlas. The Oued Tassaoute is regarded as the most significant and major tributary of the Oum Er-Rbia. This geographic area has a surface area of 1418.35 km^2 and a perimeter of 246 km. It is located 35 km from Demnate and 90 km from Marrakech. The altitude varies from 809 to 3910 m between the northern latitudes of 31°33′56″ and 31°64′47″ and the western longitudes of 6°48′40″ and 7°33′40″. Table 1 describes the characteristics of the Tassaoute watershed.

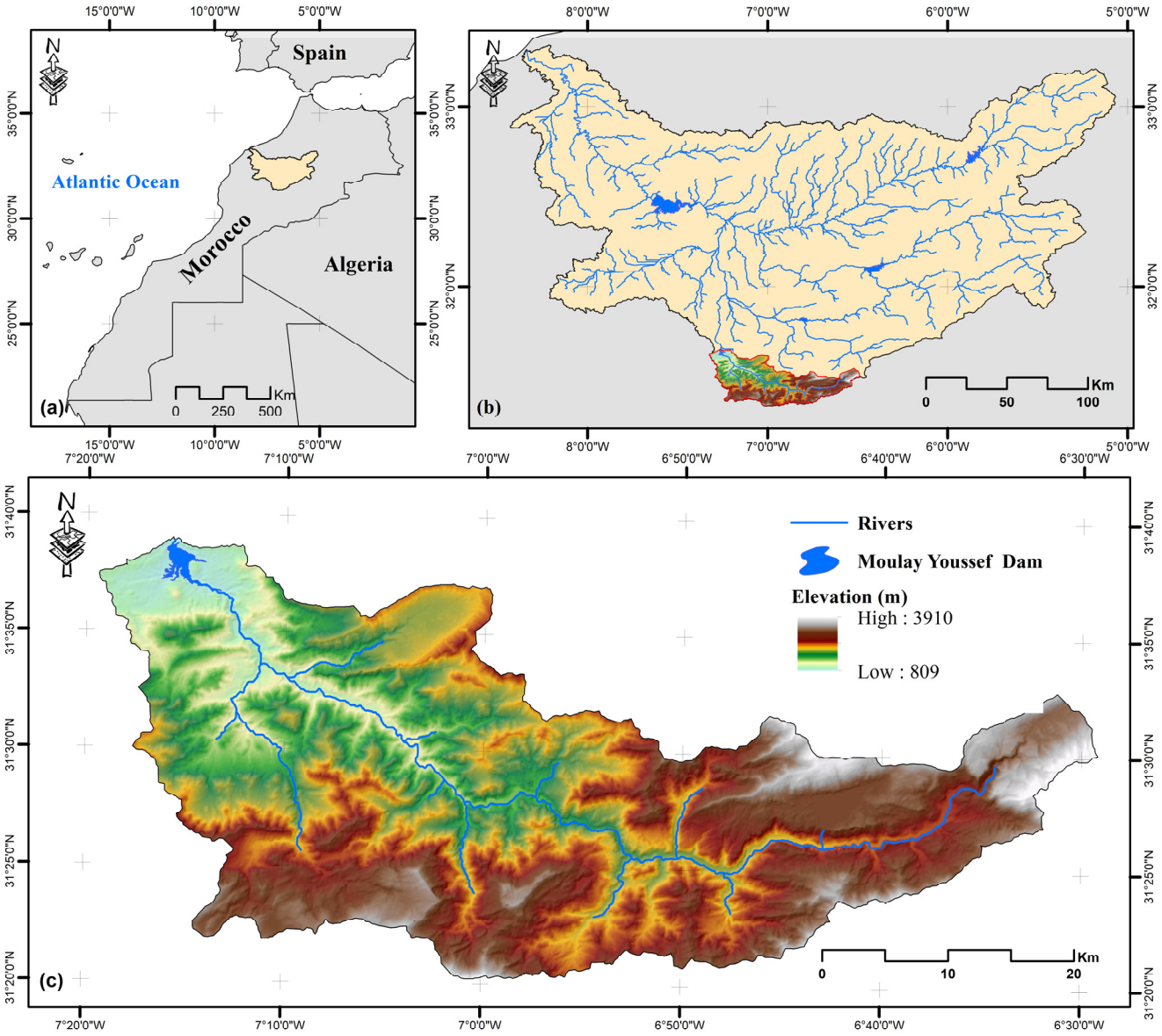

Figure 1. The geographical location of the research region; (**a**) on Moroccan scale, (**b**) on Oum Er-Rbia watershed scale, and (**c**) digital elevation model of the Tassaoute catchment (upstream of the Moulay Youssef Dam).

Table 1. Basic characteristics of Tassaoute catchment.

Parameters	Units	Values
Area	km^2	1418.35
Perimeter	km	246
Gravelius Index	–	1.83
Average elevation	m	2144.13
Elevation min	m	809
Elevation max	m	3910
Average slope (Roche)	%	1.56
Length of longest stream	km	106.9
Average stream slope	m/km	28.9
Hydrographic density	Km^{-2}	4.12
Water flow velocity	m/s	2.8

Geologically, the catchment is situated between the Jurassic massif in the east of Azilal and the Western High Atlas, which is composed of sedimentary, igneous, and metamorphic older Permian materials. The Permo–Triassic and Lias geological series are the most prevalent in the basin, whereas some formations, other than the Quaternary, are only present in small synclines.

2.2. EURO-CORDEX Initiative Climate Models

In this study, we employed five recent climate models from the EURO-CORDEX experiment [23] with 0.11° spatial resolution, listed in Table 2.

Table 2. EURO-CORDEX simulations applied in this research.

GCM	RCM	Resolution
CNRM ECEARTH IPSL MPI HAD	SMH11	12.5 km

Each model contains four different simulations:

- EVAL (evaluation simulation) is considered as a control period, using the ERA Interim reanalysis data as a boundary condition [24]. The simulation covers the period 1970–2005.
- HIST (historical run) is a control period considering the historical runs of the GCM models. The covered period is 1950–2005.
- RCP4.5 (representative concentration pathway) is the climate change scenario that conforms to +4.5 Wm^{-2} radiative forcing; it is considered as the optimistic scenario. RCP4.5 covers the period 2006–2100.
- RCP8.5 is the pessimistic scenario with additive radiation of +8.5 Wm^{-2}. The scenario covers the same period as RCP 4.5.

In this study, we extracted 16 grid cells of the five RCMs to cover the region. The projections concern two periods: 2030–2060 and 2061–2090, under the two scenarios, RCP 4.5 and RCP 8.5.

2.3. Projected Daily Changes in Precipitation and Temperature

The RCM outputs must be post-processed to examine future variations in precipitation and temperature. In order to achieve consistency with the RCMs' spatial resolution, we spatially interpolated the observed precipitation using the IDW method at a resolution of 0.11° on a monthly time scale. The same process was followed for the temperature data.

For the downscaling method, we chose the perturbation method for this work, because the RCMs' coarse resolution makes it unable to perform bias-correction techniques effectively. This approach is based on applying a climate change factor to the observed data. In the aim to model the potential variations in climate patterns, specifically changes in temperature and precipitation, these factors are derived between the historical (1985–2005) and future simulation periods (2030–2060 and 2061–2090) of each RCM, and afterward applied to the observed time series of each pixel. In this study, we employed the "delta change" method, which does not require bias correction of the RCM model [25–28]. After these processes, the corrected data were converted into a yearly time scale.

2.4. Erosion Potential Model (EPM)

The EPM is employed in this research to assess soil erosion in the High Atlas of Morocco at the present time and at the end of the century under a high-emission climate change scenario. The model takes into consideration a number of variables, including rainfall, temperature, terrain, land cover, and soil type, all of which have an impact on soil erosion.

The EPM [29–31], generally recognized as the Gavrilovic method, is a common empirical method utilized to estimate sediment output and soil loss severity on a catchment scale. The technique tries to estimate the soil loss due to water erosion and to suggest practices to minimize soil degradation. It can estimate the different types of erosion (sheet erosion, gully erosion, badlands, etc.), which make them distinct from the universal soil loss equation (USLE, RUSLE), which only applies to sheet erosion.

The method considers six individual factors: lithology and soil properties, topographic characteristics, climate conditions, land use, and observed erosion process. The calculation of the erosion coefficient (Z) of a catchment is obtained by the formulae:

$$W = \pi * T * H * \sqrt{Z^3} * F \quad (1)$$

where:

W: average annual soil erosion ($m^3/km^2/year$).
T: temperature coefficient

$$T = (0.1 * to) + 0.1 \quad (2)$$

where:

to: average annual temperature in °C.
H: average annual precipitation in mm.
F: catchment area in km^2.
Z: potential erosion coefficient.

$$Z = Y * Xa \left(\delta + \sqrt{Ja}\right) \quad (3)$$

where:

Y: coefficient of soil erodibility. It depends on the lithology, soil characteristics, and climate.
Xa: soil protection coefficient against influences related to atmospheric phenomena.
δ: coefficient that expresses the type and degree of evolution of visible erosion processes in the catchment.
Ja: slope angle (%).

To determine the Xa-Factor values, the soil protection coefficient was determined using the modified NDVI ($XaNDVI$), based on the methodology proposed by Zorn and Komac (2008) [32], the Xa-Factor is determined as follows (4):

$$Xa = (Xa.NDVI - 0.61).(-1.15) \quad (4)$$

The soil protection coefficient (Xa) was assessed using the EPM Guide Table 3 [33]. This technique categorizes land uses into six groups and estimates the coefficient 'Xa' from 0.1 (for high-density woodlands) to 1.0 (for badlands).

Table 3. EPM Soil protection coefficient values.

Coefficient of Soil Cover	Xa Factor
Mixed and dense forest	0.05–0.20
Thin forest with grove	0.05–0.20
Coniferous forest with little grove, scarce bushes, bushy prairie	0.20–0.40
Damaged forest and bushes, pasture	0.40–0.60
Damaged pasture and cultivated land	0.60–0.80
Areas without vegetal cover	0.80–1.00

Coefficient φ represents the severity of erosion processes reflected in the area, with values between 0.1 and 1 [33] (Table 4). The determination of φ factor (soil resistance to

erosion) was realized based on the proposed framework by Zorn and Komac (2008) [32], according to Formula (5):

$$\delta = \sqrt{\frac{TM4}{Qmax}} \quad (5)$$

where:

TM4 is the Landsat image band 4,
Qmax is the maximum radiance of band 4,

The erosion coefficient values in the catchment upstream of the Tassaoute, varying between 0.29 and 0.60.

Table 4. EPM coefficient values of erosion coefficient.

Coefficient of Type and Extent of Erosion	δ
Slight erosion on the catchment	0.10–0.20
20–50% of the catchment area has erosion in rivers and streams	0.30–0.50
Erosion in rivers, gullies, and alluvial deposits, karstic erosion	0.60–0.70
50–80 percent of drainage basin is impacted by surface erosion and landslides.	0.80–0.90
Erosion affect entire catchment	0.90–1.00

This study was performed in accordance with the process shown below (Figure 2).

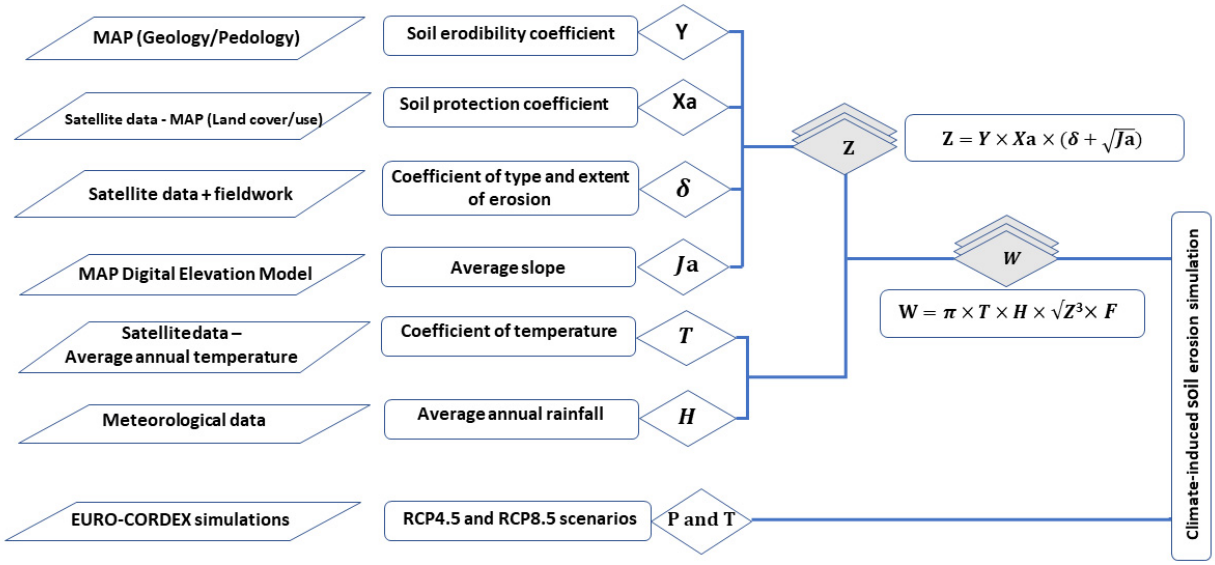

Figure 2. Flowchart of the methodology EPM climate simulation EURO-CORDEX approach.

3. Results and Discussion

3.1. Estimation of Actual Soil Losses According to the EPM Model

The map of soil loss is obtained by combining the various factors of Gavrilovic's EPM equation and accounting for the numerical values of the seven factors (Figure 3). Using the Gavrilovic method, the EPM model's quantitative results for erosion severity (coefficient Z) were mathematically evaluated by solving Equation (3); the results were then categorized into five groups to produce the erosion potential map (Table 5, Figure 3g). The areas with $Z > 1$ have a very high potential for erosion, whereas $Z < 0.2$ regions have a low erosion potential. Using Equations (1) and (2), it was predicted that the annual specific production of sediment per km^2 would be, on average, m^3/year (W) (1). Then, Equation (1) was used

to determine the erosion volume (W). Using the EPM model, the created map of W for the Tassaoute catchment was finally classified into six erosion categories (very low (tolerable), low, moderate, high, very high, and extreme) (Figure 3h).

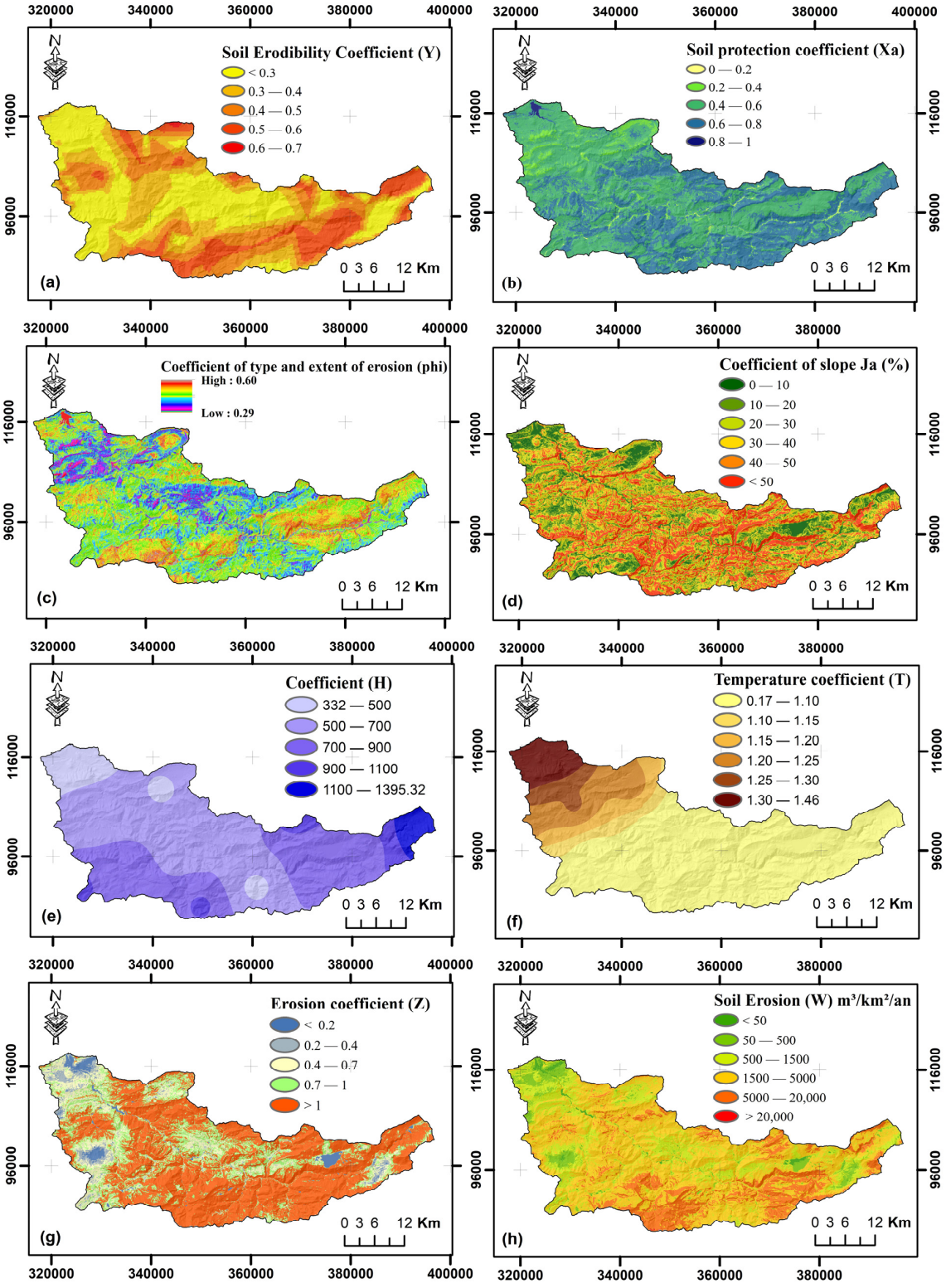

Figure 3. Spatial distribution of EPM parameters; (**a**) soil erodibility coefficient, (**b**) soil protection coefficient, (**c**) type and extent of erosion coefficient, (**d**) topographic coefficient, (**e**) Rainfall-H factor, (**f**) temperature coefficient, (**g**) potential erosion coefficient, and (**h**) soil loss.

Table 5. Potential erosion coefficient.

Potential Erosion Coefficient	Classes of (Z)	Area (km^2)	Area (%)
Very slight erosion	<0.2	41.34	2.91
Slight erosion	0.2–0.4	59.67	4.21
Medium erosion	0.4–0.7	195.17	13.76
Severe erosion	0.7–1	277.41	19.56
Excessive erosion	>1	844.76	59.56

The estimated global potential erosion average for the Tassaoute catchment from 1976 to 2005 is 3129.74 $m^3/year/km^2$. The losses per plot range from 26,321 $m^3/year/km^2$, at the maximum, to 0.24 $m^3/year/km^2$ at the minimum, and the annual soil loss was found to be equal to 3,840,670 $m^3/year$.

According to the effects of different physical and anthropogenic variables that regulate the erosive process, the erosion severity differs from one watershed region to another. These units are divided into six classes to improve the readability of the map (Figure 3 and Table 6).

Table 6. Soil loss values in the Tassaoute catchment.

Erosion Categories	Classes of (W) $m^3/year/km^2$	Area (km^2)	Area (%)
Very low (tolerable)	<50	14.68	1.03
Low	50–500	85.73	6.04
Moderate	500–1500	298.09	21.02
High	1500–5000	757.39	53.40
Very high	5000–20,000	262.17	18.48
Extreme	>20,000	0.29	0.02

Land losses greater than 1500 $m^3/year/km^2$ (high to extreme intensity class) come from 72% of the catchment zone, situated largely in the center and southeastern area of the catchment. It demonstrates how widely the phenomenon has spread. The very low to low classes (soil losses of less than 500 $m^3/year/km^2$) encompass a negligible part of the research region (7%) downstream of the catchment area and to the northwest of the basin near the Moulay Youssef Dam, and 21% of the total area has losses of between 500 and 1500 $m^3/year/km^2$ (moderate intensity class).

3.2. The Influence of Erosion Factors on Soil Loss

The considerable diversity of each erosion factor's effects leads to an uneven distribution of soil loss throughout the catchment area. Some noteworthy tendencies may be seen in the statistical association between the different parameters and the erosive dynamics (Figure 4). First of all, the 0.95 correlation between the prospective erosion map and the EPM map should be noted.

The soil resistance and slope have the biggest effects on potential erosion. In the case of the erosion map, precipitation (correlation coefficient = 0.66) is the most important factor in the erosive dynamics, and then soil resistance and slope (correlation coefficients = 0.63 and 0.58 respectively), followed by the soil protection factor, and, finally, the soil regularization factor.

More highly correlated with the soil resistance factor is the degree of visible erosion. Precipitation seems to have a higher negative correlation with temperature (−0.84). None of the other factors appear to have an impact on the slope, erosion types, and soil protection.

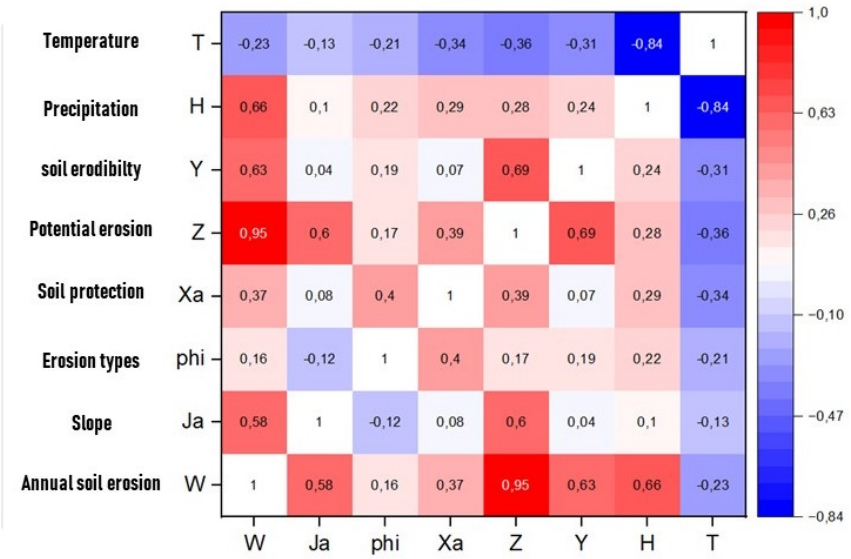

Figure 4. Pairwise Pearson's correlation between soil erosion rate and input factors.

3.3. Future Projections in Precipitation and Temperature

3.3.1. Future Projections Using All Models

The future temperatures and precipitation are predicted using five models under two climate change scenarios, RCP4.5 and 8.5 (Figures 5 and 6). Regarding annual precipitation, there is a significant difference between the models' projected quantities. In fact, model MPI predicted the greatest values for the period 2030–2060, with a minimum of 433 mm/year and a maximum of 1810 mm/year, whereas model IPSL forecasted lower values, with a minimum of 110 mm/year and a maximum that does not surpass 437 mm/year. As for the 2060–2090 period, model MPI still predicts the highest precipitation in the catchment area, amounting to 1770 mm/year, while model IPSL is the most pessimistic, with values ranging from 70 to 229 mm/year (Figure 5).

The findings of the temperature prediction indicate, from a more general standpoint, that there is a significant difference between the values (minimum, maximum, and average) of the five models used in this study, on the one hand, and between the scenarios, on the other hand. Indeed, taking into account the first period (2030–2060), the most optimistic prediction is that of model ECEARTH, with a minimum value of 1.58 °C and a maximum of 22.1 °C. The most pessimistic prediction is made by model IPSL (min = 9.25 °C and max = 24.9 °C). For the period 2060–2090, the same models consistently provide optimistic (model ECEARTH with min = 3.25 °C and max = 22.6 °C) and pessimistic (model IPSL with min = 13.9 °C and max =28.3 °C) forecasts (Figure 6).

3.3.2. Averaged Values of Projected Precipitation and Temperature (Figures 7 and 8)

Figure 7 shows the monthly projected precipitation, averaged over the basin, from the ensemble of the five models under the two RCP scenarios compared to the historical precipitation. The result indicates that precipitation shows a pronounced decrease with −32% and −46% under RCP4.5 for the periods 2030–2060 and 2061–2090, respectively, and −28% and −56% under RCP8.5 for the same periods, respectively. This decrease in the precipitation amount is pronounced during both scenarios for the two periods (Figure 9). However, the decrease is less pronounced during the autumn season, due to the intense events of precipitation that can occur in the future [34]. These results are in parallel with recent papers about Morocco, where [26,34] found that, in the center of Morocco, the decrease in precipitation will be around −20%.

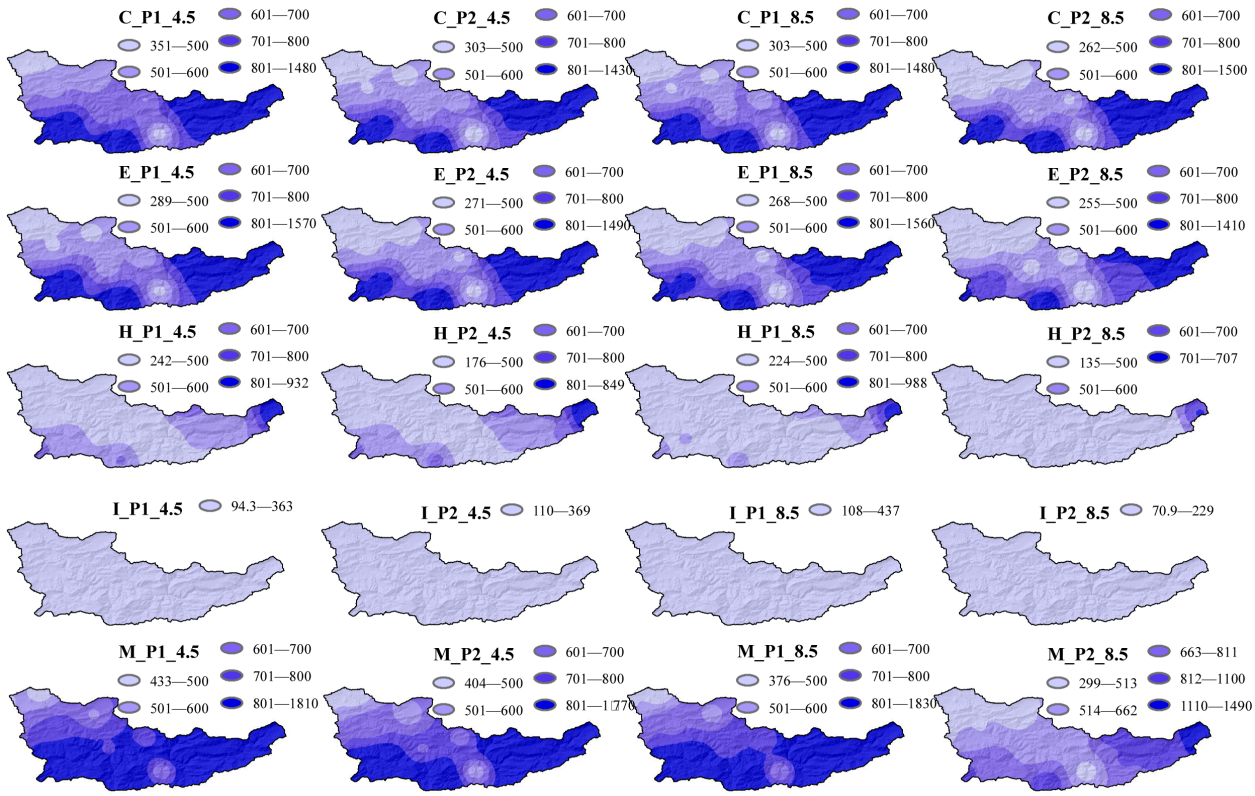

Figure 5. Future changes of precipitation of the RCMs under RCP4.5 and RCP8.5 for the periods 2030–2060 and 2061–2090. C: CNRM, E: ECEARTH, H: HAD, I: IPSL, M: MPI, and P: period.

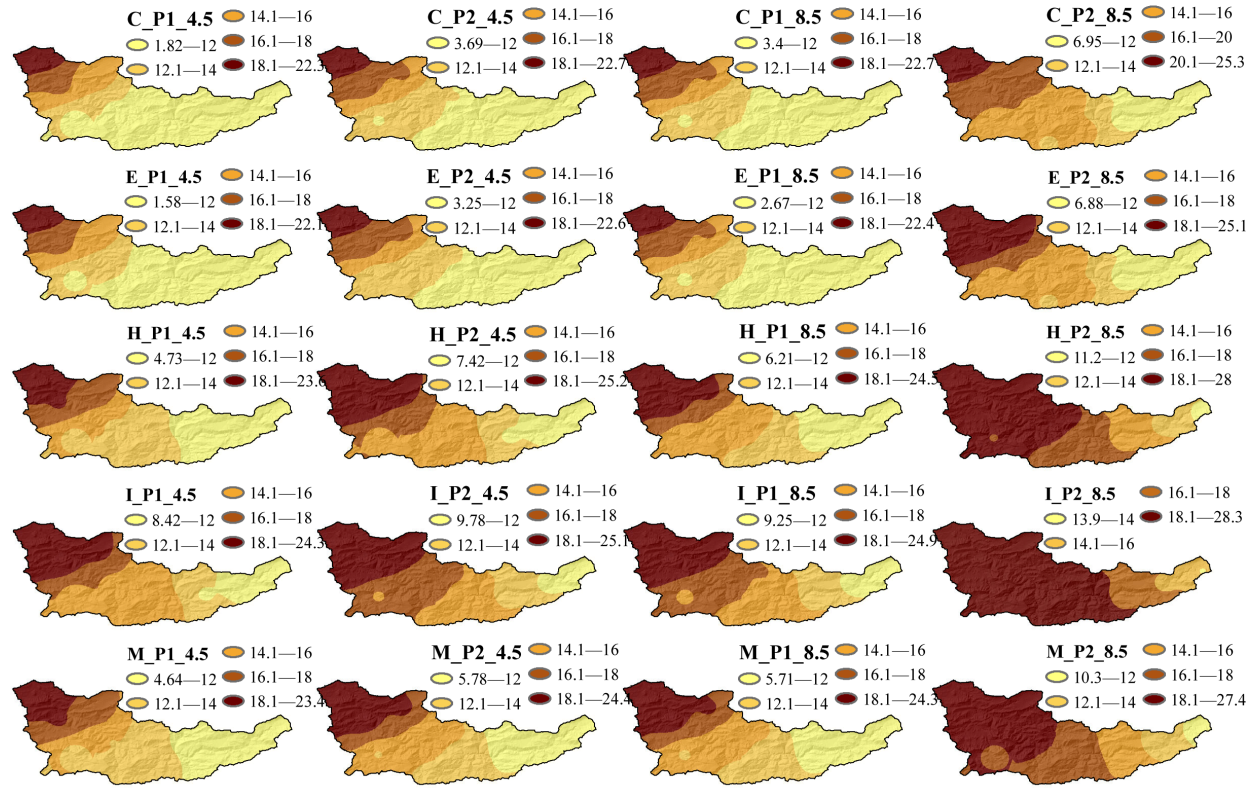

Figure 6. Future changes of temperature of the RCMs under RCP4.5 and RCP8.5 for the periods 2030–2060 and 2061–2090. C: CNRM, E: ECEARTH, H: HAD, I: IPSL, M: MPI, and P: period.

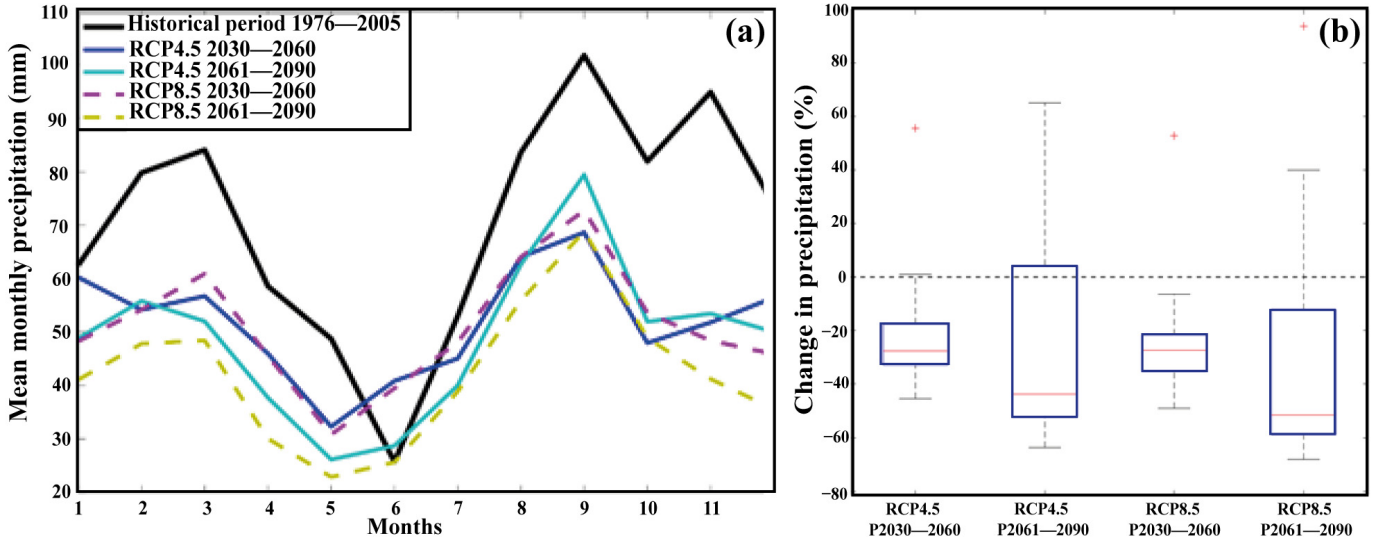

Figure 7. Future projected monthly precipitation (**a**) and future changes in precipitation by scenario and period (**b**).

Figure 8 illustrates the expected temperature cycle, based on the two RCP scenarios for the two periods. Figure 8b displays, in absolute temperature values, the effect of climate change for each RCP scenario and period. Both scenarios detect a large increase in temperature, as is evident. The temperature projections, on average, are +2.8 °C and 4.1 °C for the RCP4.5 scenario and +3.1 °C and +5.2 °C for the RCP8.5 scenario, for the periods 2030–2060 and 2061–2090, respectively. These results are in parallel with [35], where they found an increase in temperature in the Oum Er-Rbia basin from +1.9 °C to +3 °C under RCP4.5 and +4 °C to +6.1 °C under RCP8.5. Compared to precipitation, these variations are rather consistent throughout the year, with a higher rise during the summer months. Summer has essentially little runoff or snow cover; therefore, summer temperature changes are unlikely to have a significant influence on flows. However, increases in winter and spring temperatures might have a significant impact on the snow, decreasing the time of snow cover and, consequently, the available snow volume.

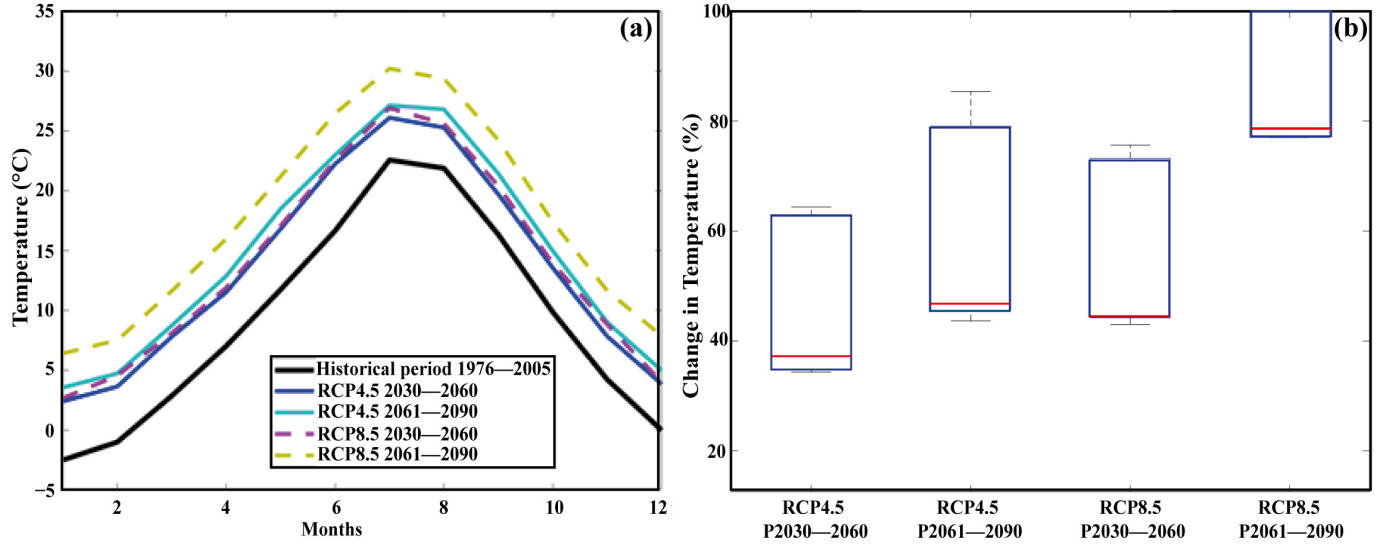

Figure 8. Future projected daily temperature (**a**) and future changes in temperature by scenario and period (**b**).

In addition, we spatially interpolated the forecasted temperature coefficients and precipitation data to highlight regional variability at the catchment level (Figure 9) The precipitation values indicate that the eastern portion of the basin (which is downstream) will receive less precipitation than the western portion (which is upstream). During the period 2030–2060, the values will vary depending on the scenario, with a minimum of 264 mm/year and a high of 1226 mm/year under the RCP4.5 scenario, and a minimum of 236 mm/year and a maximum of 1260 mm/year under the RCP 8.5 scenario (Figure 9a,b). The maximum values for the second period (2060–2090) will not exceed 1044 mm/year under scenario RCP8.5 and 1169 mm/year under scenario RCP4.5 (Figure 9c,d).

Concerning the temperature coefficient, T, the first period (2030–2060) demonstrates higher values downstream (0.72 and 0.80 for RCP4.5 and 8.5, respectively) than upstream (1.55 and 1.57 as maximum values for RCP4.5 and 8.5, respectively) (Figure 9e,f). Looking further into the future (period 2060–2090), the projections indicate a significant increase in the coefficient, particularly under the pessimistic scenario (min = 1.04 and max = 1.67), with the class of 1.30–1.67 covering the majority of the catchment area (Figure 9g,h).

All of these findings illustrate the projected impact of climate change on the spatial and temporal variability of annual precipitation and temperature in this semiarid mountainous region. Therefore, the region is quite vulnerable to these fluctuations, which will certainly affect the anticipated soil loss rates.

3.4. Projected Soil Erosion Rates

The method presented in Section 2.2 was used to obtain projected rainfall data, which were then utilized to estimate annual average precipitation (H) for each scenario. Then, according to the procedure outlined, the mean annual temperature map was created by taking into account each potential future scenario (RCP 4.5, and RCP 8.5). These maps were used to solve Equation (2) and produce the temperature coefficient (T) maps depicted in Figure 7. Then, we performed the used model to estimate soil losses in the future, with a static land cover to assess the impacts of climate change on soil erosion, irrespective of changes in land cover.

3.4.1. Projected Soil Erosion Rates Using All Models

Figure 10 depicts the predictions of erosion rates using the EPM model for each model (ECEARTH, IPSL, MPI, and HAD), scenario (RCP4.5 and RCP8.5), and time period (2030–2060 and 2060–2090). Comparing the models, it appears that models CNRM, ECEARTH, and MPI forecast extremely high rates, whereas model IPSL predicts the lowest rate. In fact, the estimated rates for the years 2030–2060 under the RCP4.5 scenario range from 0–37,014, 0–37,621, 0–29,120, and 0–56,952 $m^3/year/km^2$ for models CNRM, ECEARTH, HAD, and MPI, respectively, while model IPSL predicts the lowest rates, which will not exceed 13,233 $m^3/year/km^2$. Nevertheless, under the pessimistic scenario (RCP8.5), the rates will rise to 59,514 $m^3/year/km^2$ (model MPI) and 42,077 $m^3/year/km^2$ (model CNRM). For the period 2060–2090, model CNRM predicts a significant increase in rates, with maximum values of 42,077 $m^3/year/km^2$ under RCP4.5 and 51,615 $m^3/year/km^2$ under RCP8.5. Also, models ECEARTH and MPI forecast continuously high rates, ranging between 0–40,723 (RCP4.5) and 0–48,302 (RCP8.5), 0–59,600 (RCP4.5), and 0–59,472 (RCP8.5) $m^3/year/km^2$, respectively. However, models HAD and IPSL predict an increase in soil losses under the RCP4.5 scenario, with maximum values reaching 30,212 and 20,000 $m^3/year/km^2$, respectively, whereas, under the pessimistic RCP8.5 scenario, the soil losses decrease significantly, with maximum values reaching only 28,794 and 10,837 $m^3/year/km^2$ (model HAD and model IPSL, respectively) (model IPSL).

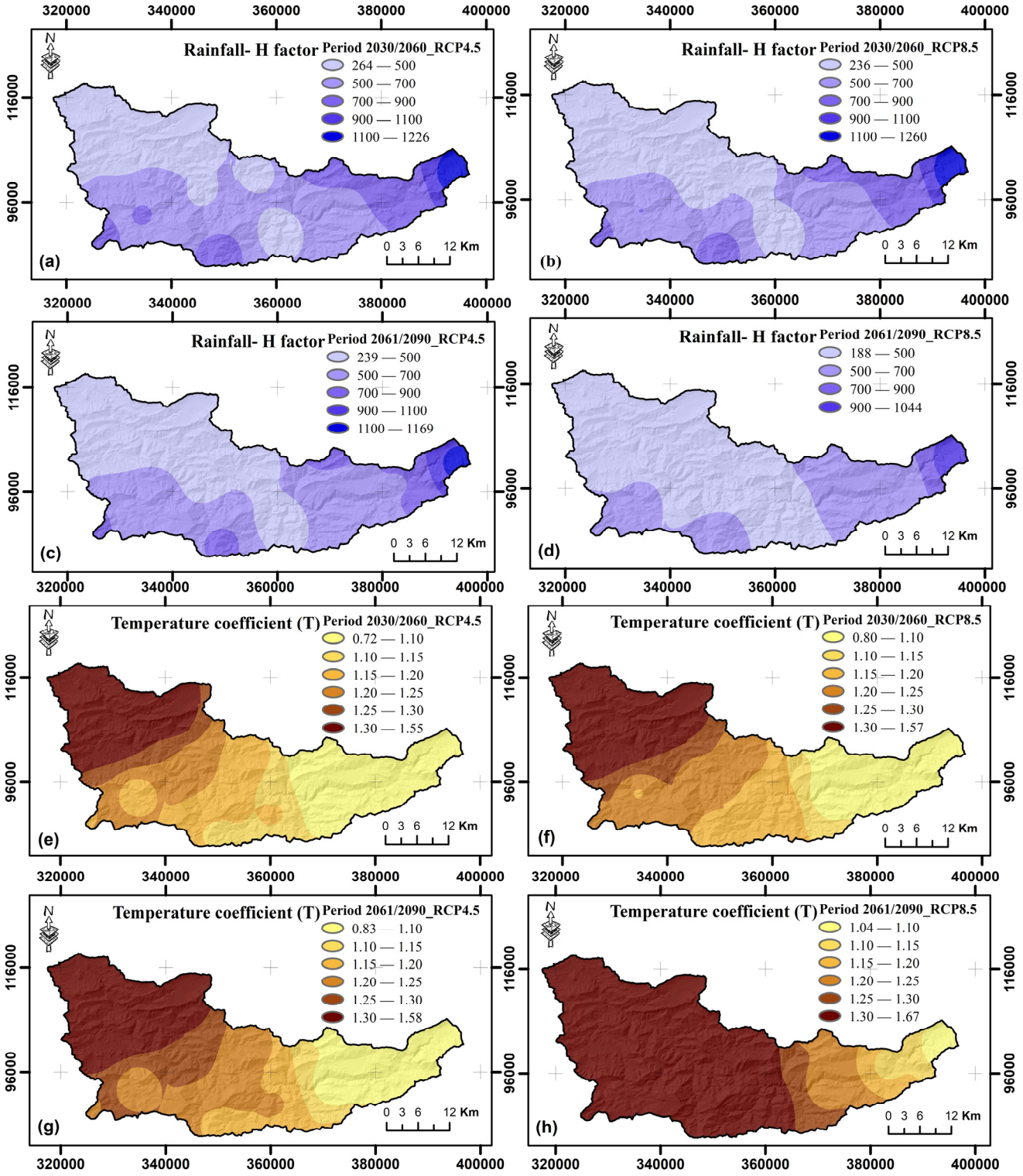

Figure 9. Maps of average annual precipitation (Rainfall-H factor) and temperature coefficient (T) considering future scenarios RCP 4.5 and RCP 8.5. (**a**) period 2030–2060 RCP4.5, (**b**) period 2030–2060 RCP8.5, (**c**) period 2061–2090 RCP4.5, (**d**) period 2061–2090 RCP8.5, (**e**) period 2030–2060 RCP4.5, (**f**) period 2030–2060 RCP8.5, (**g**) period 2061–2090 RCP4.5, (**h**) period 2061–2090 RCP4.5.

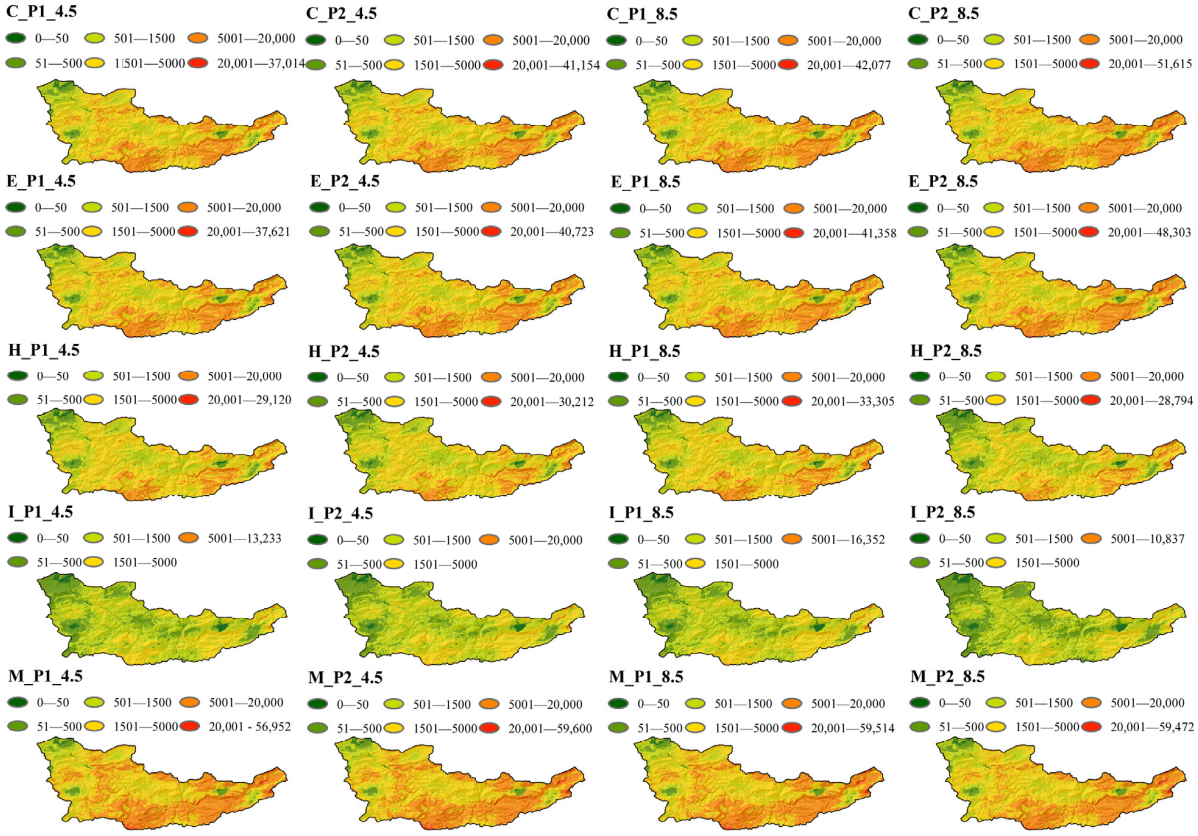

Figure 10. Soil erosion rates of the RCMs models under RCP4.5 and RCP8.5 for the periods 2030–2060 and 2061–2090. C: CNRM, E: ECEARTH, H: HAD, I: IPSL, M: MPI and P: period.

These results enabled us to calculate the change rates for the minimum and maximum values (Table 7). Consequently, the table demonstrates an increase in soil loss rates across all time periods and scenarios. In fact, for the first period (2030–2060) under scenario RCP4.5, the average maximum values of the five models will increase by approximately 10,981.94 $m^3/year/km^2$ (46.13%) compared to the initial value (baseline). The situation becomes more serious under the RCP8.5 scenario, where the maximum losses reach 61.81% (14,714.94 $m^3/year/km^2$). For the second period (2060–2090), and across the two scenarios, the change rates reach 56.59% (about 13,472 $m^3/year/km^2$) for the maximum losses under the RCP4.5 scenario. Moreover, the change is approximately 67.2% (15,997.94 $m^3/year/km^2$) for the maximum losses under the RCP8.5 scenario.

Table 7. The minimum, maximum, and average values of expected soil losses.

Baseline	**W ($m^3/Km^2/year$)**					
Min	0					
Max	23,806.06					
Scenario				**RCP 4.5**		
Periods		**2030—2060**			**2060—2090**	
	W ($m^3/Km^2/year$)	ΔW	ΔW %	W ($m^3/Km^2/year$)	ΔW	ΔW %
Min	0.00	0.00	0.00	0.00	0.00	0.00
Max	34,788.00	+10,981.94	+46.13	37,278.40	+13,472.34	+56.59
Scenario				**RCP 8.5**		
Min	0.00	0.00	0.00	0.00	0.00	0.00
Max	38,521.00	+14,714.94	+61.81	39,804.00	+15,997.94	+67.2

3.4.2. Averaged Projected Soil Erosion Rates

The annual soil loss (m^3/year) and catchment erosion rate (m^3/km^2/year) were calculated using the previously specified factors and the EPM technique for the baseline (1976–2021) and future periods (2030–2060/2061–2090), taking into consideration two distinct future scenarios (RCP4.5 and RCP8.5) and a static land cover (Figures 11 and 12). Lastly, the findings were compared in order to quantify the effects of climate change on soil erosion.

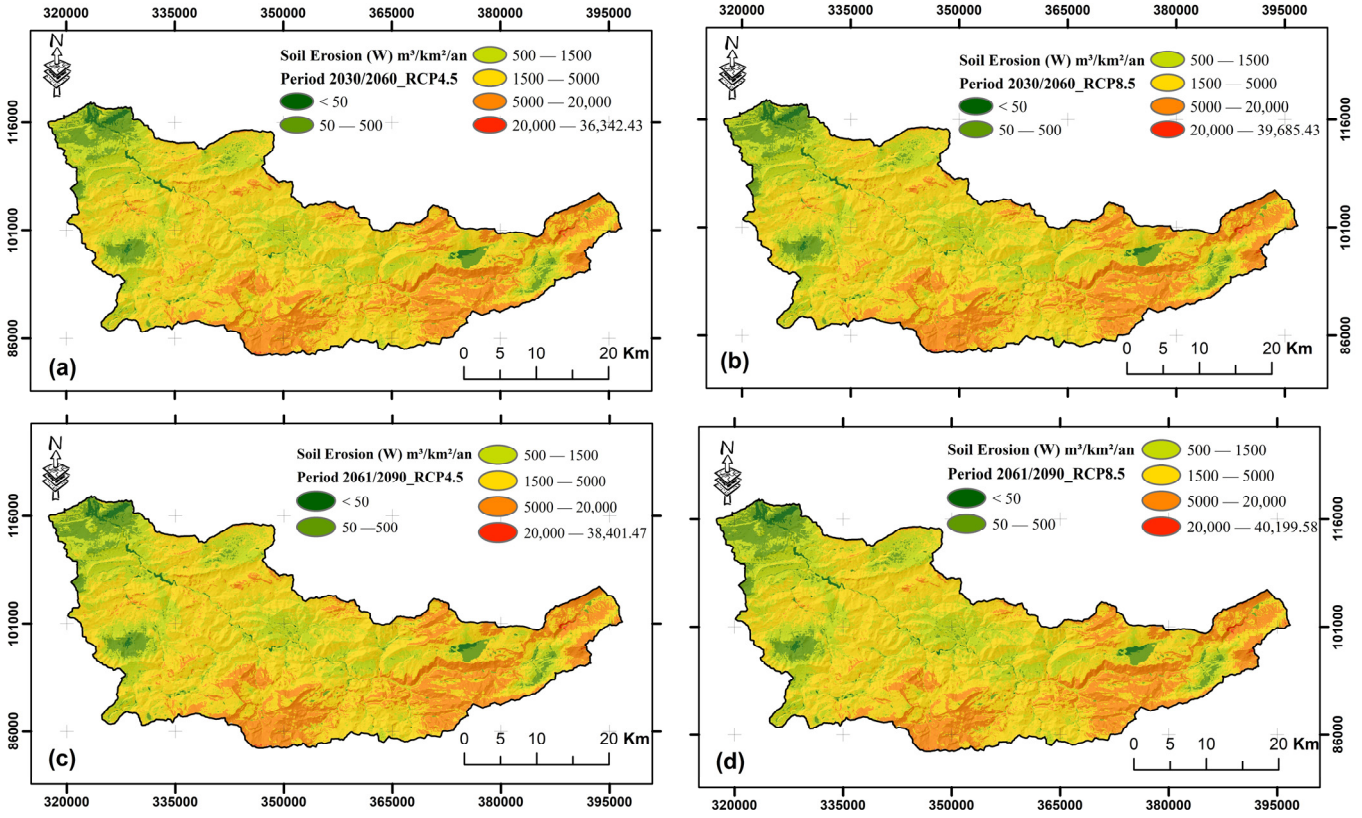

Figure 11. Maps of average annual soil erosion (W) [$m^3/year/km^2$] considering future scenarios RCP4.5, RCP8.5, and using the EPM model. (**a**) period 2030–2060 RCP4.5, (**b**) period 2030–2060 RCP8.5, (**c**) period 2061–2090 RCP4.5, (**d**) period 2061–2090 RCP8.5.

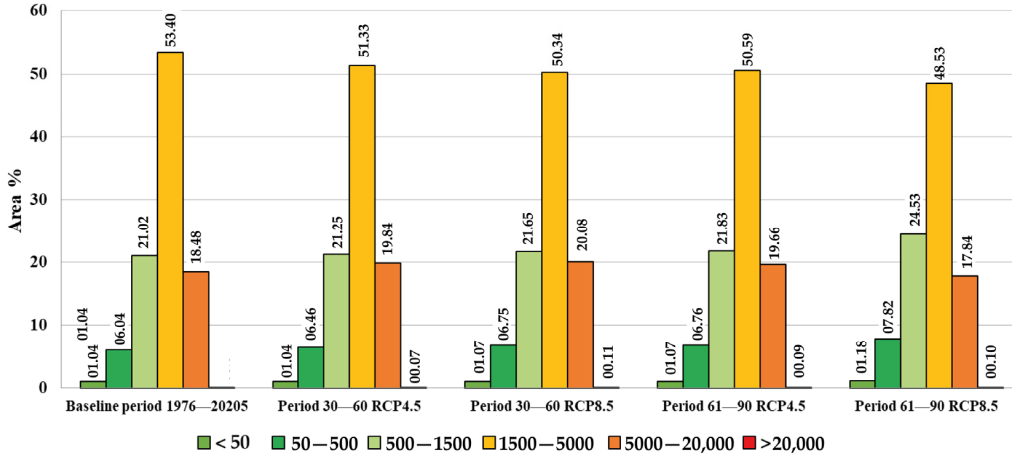

Figure 12. Classes of the change in the erosion rate from the present circumstances to the end of the 21st century, under the two scenarios, RCP4.5 and RCP8.5.

The findings (Table 8) show that the total soil loss would be elevated by 137,738 m^3/year, 176,789 m^3/year, and 107,885 m^3/year for the periods RCP4.5/2030–2060, RCP8.5/2030–2060, and RCP4.5/2061–2090, respectively, and, as a result, the erosion rate would be elevated by 97.11 m^3/km^2/year, 124.64 m^3/km^2/year, and 76.06 m^3/km^2/year, in the same order. However, the RCP8.5/2061–2090 scenario suggests a 175,612 m^3/year reduction in total soil loss and 123.82 m^3/km^2/year in the erosion rate. Table 8 summarizes the detailed findings for the present and future climates.

Table 8. Annual soil loss and erosion rate in the current and projected climates.

Period/Climate Change Scenario		Soil Loss (m^3/year)	Change (m^3/year)	Erosion Rate (m^3/year/km^2)	Change (m^3/year/km^2)	Change (%)
1976–2021		4,439,067		3129.74		
2030–2060	RCP4.5	4,576,805	+137,738	3226.85	+97.11	+3.10
	RCP8.5	4,615,856	+176,789	3254.38	+124.64	+3.98
2061–2090	RCP4.5	4,546,952	+107,885	3205.80	+76.06	+2.43
	RCP8.5	**4,263,455**	**−175,612**	**3005.92**	**−123.82**	**−3.96**

To examine the influence on the spatial variation of erosion rates, Figure 12 illustrates the classes of the variation in the erosion rate from the present condition to the end of the 21st century, in view of the two climate change scenarios, RCP4.5 and RCP8.5. Clearly, the areas occupied by the classes with soil loss rates below 5000 m^3/km^2/year will decrease significantly in comparison to the classes with soil loss rates beyond this threshold. In fact, the soil losses between 500–5000 m^3/km^2/year will decrease from 53.40% of the total basin surface in the baseline period to 51.33% in the period 2030–2060 under the RCP4.5 scenario, to 50.34% under the RCP8.5 scenario and to 50.59% for the period 2060–2090 under the RCP4.5 scenario, and to 48.53% under the most pessimistic scenario, RCP8.5, by the year 2090. However, the loss rates in excess of 5000 m^3/km^2/year will increase significantly, particularly in the first period under the two scenarios.

In addition, in order to highlight the spatial variability of the change rates under different scenarios in the two time periods (Figure 13), we have spatialized these changes by calculating the difference between the expected losses for each period and those of the baseline period. Consequentially, the modeling results indicated that, in high-altitude regions and notably upstream of the catchment, erosion rates might significantly increase under the considered climate change scenarios.

In terms of the Mediterranean region's future climate conditions [36–39], and especially Morocco, a warmer and dryer climate is anticipated. Furthermore, an increase in temperature of between +2 °C and +5 °C is anticipated in Morocco, despite the fact that there would be a −20% decrease in precipitation in the center of Morocco [34]. In addition, according to a review of the literature, future soil erosion will be affected by climate change. However, all the previous research has shown that the projected soil erosion patterns in the studied areas could be extremely heterogeneous. Our research substantially supports these findings, confirming an overall rise in soil erosion in the catchments of the Atlas Mountains caused by climate change, modulated particularly by rainfall as a determining factor that can lead to regional patterns of increasing erosion. The definition of a general trend becomes very difficult, as a result. In comparison to other catchments in the Atlas Mountains, the rate of erosion in the research region was assessed to be rather high. The weak geological subsurface and steep slopes, in addition to the degraded forest cover, were shown to enhance the development of erosion phenomena. Concerning the estimated erosion rates for the baseline period (3129 m^3/km^2/year on average), they are quite equivalent to those determined by [40–42] in the Moroccan context. In addition, it was revealed that, although precipitation will decrease, the soil loss rates will continue to rise [43,44], particularly in the first period between 2030 and 2060. This can be explained by the fact that, even if the annual rainfall in the basin decreases in quantity, taking into account its spatial variability, it is clear that the maximum values expected will be localized in the upstream

portion of the basin and coincide with the areas most susceptible to high loss rates, due to their high exposure resulting from their degraded vegetation cover with significant slopes. On the Mediterranean scale, [45] the research confirms similar losses in an Italian river basin, as well as a tendency of change in loss between 6 and 10% by 2060, which is consistent with the results of this study. Forthmore [39] suggested an increased soil loss in a mountainous catchment in Greece.

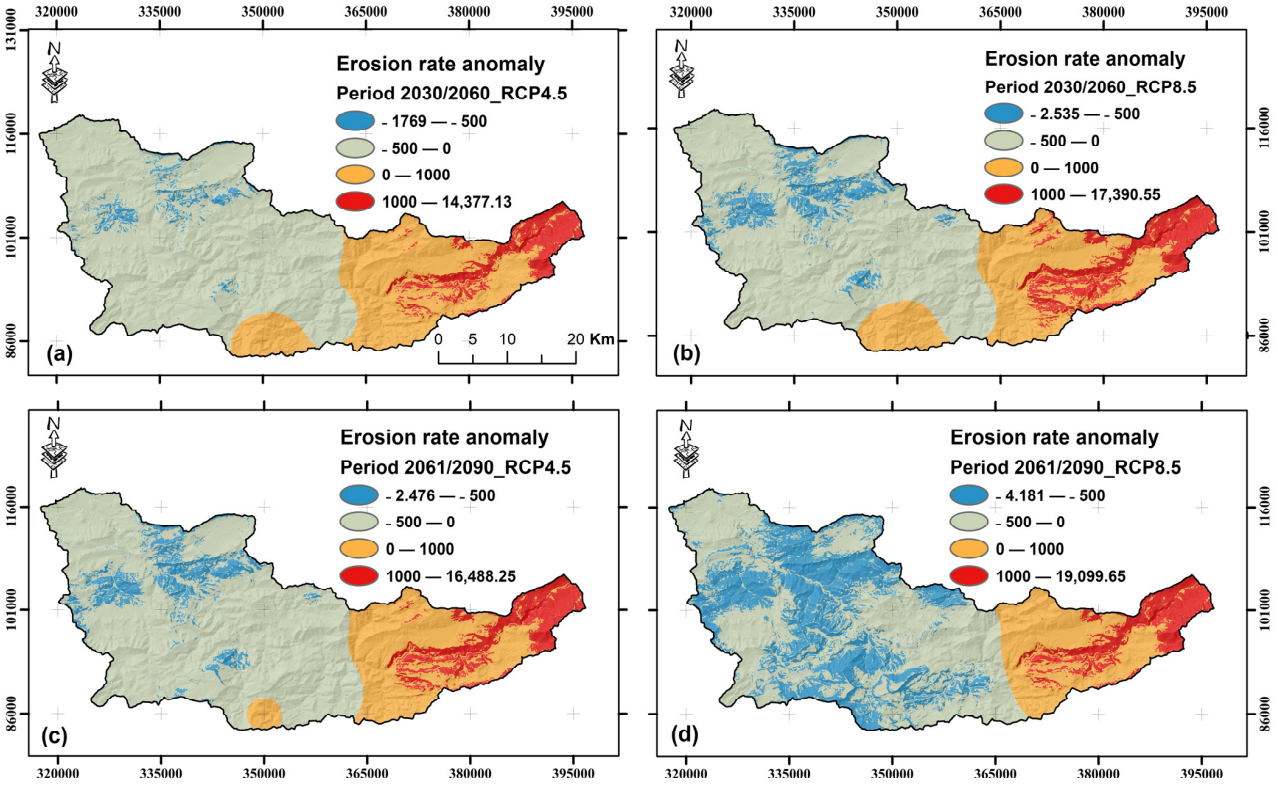

Figure 13. Anomaly of soil erosion rate relative to the baseline period (1976–2005) for the periods 2030–2060 and 2061–2090 under scenarios RCP4.5 and RCP8.5. (**a**) Period 2030–2060 RCP4.5, (**b**) period 2030–2060 RCP8.5, (**c**) period 2061–2090 RCP4.5, (**d**) period 2061–2090 RCP8.5.

Comparing the two scenarios, it appears that scenario 4.5 predicts a rise in soil loss during both time periods, with a peak in the first. In contrast, the second scenario (8.5) forecasts a substantial increase in losses during the first period and a major drop during the second. This can be attributed to the fact that the first scenario, 4.5, is more optimistic regarding the rates of change of precipitation and temperature during the initial period. In contrast, scenario 8.5 is more pessimistic, predicting a large decrease in precipitation by 2090, which will reduce the closely associated loss rates. Comparing the periods, it is evident that, given the precipitation and temperature trends, soil losses in the first period (2030–2060) are going to be greatly susceptible to the effects of climate change. In addition, the results of the three RCP 4.5 (2060 and 2090) and RCP 8.5 (2060) scenarios indicate that precipitation will fall significantly while erosion rates go up (+3%). This can be explained by the spatial component; even if precipitation on the basin scale decreases, the rates upstream of the basin maintain their high values (Figure 9a–d), and these areas coincide with the regions with degraded vegetation and steep slopes, potentially leading the EPM model to estimate high erosion rates.

These results can be a useful resource for decision-makers and long-term management. However, it is essential to recognize the limitations of the employed approaches. Certainly, there is a pressing need for accurate future climate estimates in order to plan catchment management and infrastructure projects. The regional climate model (RCM) is the most current instrument for simulating future climatic conditions. Using models, on the other

hand, might increase uncertainty with respect to a variety of key temporal and geographical scaling concerns with the input data. Generally, RCMs overestimate temperature and underestimate monthly precipitation, whereas better simulation is possible in the spring and summer for temperature data and the winter and autumn for precipitation data [36,37]. Another constraint is that the study only takes climate factors (rainfall and temperature) into account, assuming that all other factors (slope, soil erodibility, land use and land cover, and conservation practices) will remain static in the future. Soil erosion and its vulnerability may rise or fall throughout the twenty-first century depending on changes in these factors. However, the statistically based downscaling model and the EURO-CORDEX regional climate model predict that, in the future, there will be more or less rainfall, which will lead to an increase or decrease in vegetation cover, land use, and conservation practices. In addition, in general, the climate change scenarios exhibit considerable uncertainty in their projections. Finally, empirical models represent an alternative analysis tool in the absence of specific tangible data. Nonetheless, field observations, coupled with an estimation of the future evolution of additional factors influencing erosion rates, such as vegetation and human impact, could boost the accuracy and dependability of the entire process.

4. Conclusions

The climate change effect on soil degradation in a mountainous catchment in Morocco's High Atlas was investigated by means of the Gavrilovic erosion prediction method and the EURO-CORDEX regional climate model's climate simulation. The following are the major conclusions reached:

- Applying the EPM model to the hilly catchment of Tassaoute upstream, the annual soil loss was estimated to be 4,439,067 m^3/year, with an erosion rate of 3129.74 m^3/year/km^2.
- Based on the EURO-CORDEX regional climate model data, we predict a decrease in annual precipitation of −32% and −46% under RCP4.5 for the periods 2030–2060 & 2061–2090, respectively, and −28% and −56% under RCP8.5 for the same periods, respectively, and a large increase in temperature of +2.8 °C and 4.1 °C for the RCP4.5 scenario and +3.1 °C and +5.2 °C for the RCP8.5 scenarios for the periods 2030–2060 and 2061–2090, respectively.
- The model above predicted a bigger decline in monthly rainfall, particularly in the spring, and this decrease is less pronounced during the autumn season due to the intense events of precipitation that can occur in the future. In terms of temperature, summer should see a higher increase in the mean monthly temperature.
- Finally, a major increase in erosion rate was assessed, based on the described variations in climatic conditions in the study region. Similar assessments should be conducted throughout Morocco's mountainous regions in order to identify potential erosion-prone locations. Furthermore, researching how climate change would impact other hydrometeorological risks (such as floods, flash floods, landslides, etc.) is required for adaptation and mitigation. The results of the current study, using the erosion prediction model; the erosion potential model, and the climate simulation of the EURO-CORDEX regional climate model, provide estimates of climate change at a very high resolution and its influence on water -induced soil erosion. It should be the goal of future studies to show how important it is to use models with a higher resolution in areas with complicated characteristics. Simulations of better temporal scale data (e.g., daily) will possibly also be investigated.

Author Contributions: Conceptualization, A.E., E.M.E.K., A.B. and M.N.; methodology, A.E. and E.M.E.K.; software and validation, A.E., E.M.E.K., E.F., H.E., L.B.-I. and M.N.; formal analysis, A.E., E.M.E.K., M.K. and A.B.; investigation, K.Z. and M.N.; resources, Y.T. and E.M.E.K.; data curation, A.E., Y.T., E.F. and E.M.E.K.; writing—original draft preparation, A.E., E.M.E.K. and M.N.; writing—review and editing, H.E. and A.C.; visualization, L.B.-I., M.K. and K.Z.; supervision, A.B. and A.C.; project administration, A.E., E.M.E.K. and A.C. All authors have read and agreed to the published version of the manuscript.

Funding: This research was funded by the research program "MorSnow-1" (Accord spécifique n39 entre OCP S.A et UM6P).

Data Availability Statement: The datasets generated during the current study are available from the corresponding author upon reasonable request.

Acknowledgments: This research was conducted in the Data Science for Sustainable Earth Laboratory (Data4Earth). Thanks are due to the Oum Er-Rbia Hydrological Basin Agency (ABHOER) for providing the observed data, and to the MorSnow-1 research program within the UM6P (Mohammed VI Polytechnic University) for their financial support.

Conflicts of Interest: The authors declare no conflict of interest.

References

1. Baffaut, C.; Thompson, A.L.; Duriancik, L.F.; Ingram, K.A.; Norfleet, M.L. Assessing cultivated cropland inherent vulnerability to sediment and nutrient losses with the Soil Vulnerability Index. *J. Soil Water Conserv.* **2020**, *75*, 20A–22A. [CrossRef]
2. Gleeson, T.; Wang-Erlandsson, L.; Porkka, M.; Zipper, S.; Jaramillo, F.; Gerten, D.; Fetzer, I.; Cornell, S.E.; Piemontese, L.; Gordon, L.J.; et al. Illuminating water cycle modifications and Earth System resilience in the Anthropocene. *Water Resour. Res.* **2020**, *56*, e2019WR024957. [CrossRef]
3. Sposito, G. Sustaining "the Genius of Soils". In *The Soil Underfoot*; Churchman, G.J., Landa, E.R., Eds.; CRC Press: Boca Raton, FL, USA, 2014; pp. 395–408.
4. Reza, M.; Mansouri, D.; Bagherzadeh, A. Evaluation of Sediment Yield in PSIAC and MPSIAC Models by Using GIS at Toroq Catchment, Northeast of Iran. *Front. Earth Sci.* **2012**, *6*, 83–94. [CrossRef]
5. Perron, J.T. Climate and the Pace of Erosional Landscape Evolution. *Annu. Rev. Earth Planet. Sci.* **2017**, *45*, 561–591. [CrossRef]
6. IPCC. Summary for policy makers. In *Climate Change. The Physical Science Basis, Proceedings of the 10th Working Group I Session; Paris, 29 January–1 February 2007*; Solomon, S.D., Qin, M.M., Chen, M.M., Marquis, K.B., Averyt, M.T., Millers, H.L., Eds.; Cambridge University Press: Cambridge, UK; New York, NY, USA, 2007.
7. Plangoen, P.; Babel, M.S.; Clemente, R.S.; Shrestha, S.; Tripathi, N.K. Simulating the impact of future land use and climate change on soil erosion and deposition in the Mae Nam Nan sub-catchment, Thailand. *Sustainability* **2013**, *5*, 3244–3274. [CrossRef]
8. Nearing, M.A. Potential changes in rainfall erosivity in the U.S. with climate change during the 21st century. *J. Soil Water Conserv.* **2001**, *56*, 229–232.
9. Michael, A.; Schmidt, J.; Enke, W.; Deutschlander, T.; Maltiz, G. Impact of expected increase in precipitation intensities on soil loss results of comparative model simulations. *Catena* **2005**, *61*, 155–164. [CrossRef]
10. Neal, M.R.; Nearing, M.A.; Vining, R.C.; Southworth, J.; Pfeifer, R.A. Climate change impacts on soil erosion in Midwest United States with changes in crop management. *Catena* **2005**, *61*, 165–184. [CrossRef]
11. Favis-Mortlock, D.T.; Boardman, J. Nonlinear responses of soil erosion to climate change: A modelling study on the UK South Downs. *Catena* **1995**, *25*, 365–387. [CrossRef]
12. Favis-Mortlock, D.T.; Guerra, A.J.T. The implications of general circulation model estimates of rainfall for future erosion: A case study from Brazil. *Catena* **1999**, *37*, 329–354. [CrossRef]
13. Mullan, D.; Favis-Mortlock, D.T.; Fealy, R. Addressing key limitations associated with modelling soil erosion under the impacts of future climate change. *Agric. Forest. Meteorol.* **2012**, *156*, 18–30. [CrossRef]
14. Azimi Sardari, M.R.; Bazrafshan, O.; Panagopoulos, T.; Sardooi, E.R. Modeling the impact of climate change and land use change scenarios on soil erosion at the Minab Dam Watershed. *Sustainability* **2019**, *11*, 3353. [CrossRef]
15. Simonneaux, V.; Cheggour, A.; Deschamps, C.; Mouillot, F.; Cerdan, O.; Le Bissonnais, Y. Land use and climate change effects on soil erosion in a semi-arid mountainous catchment (High Atlas, Morocco). *J. Arid. Environ.* **2015**, *122*, 64–75. [CrossRef]
16. United Nations Development Programme. *Fighting Climate Change: Human Solidarity in a Divided World*; Palgrave: Macmillan, UK, 2007; pp. 1–18.
17. Ghanam, M. La désertification au Maroc et Quelle stratégie de lutte ? In 2nd FIG Regional Conference Marrakech, Morocco 2003, December 2e5. Available online: http://www.fig.net/pub/morocco/proceedings/TS4/TS4_5_ghanam.pdf (accessed on 20 October 2022).
18. Ouatiki, H.; Boudhar, A.; Leblanc, M.; Fakir, Y.; Chehbouni, A. When climate variability partly compensates for groundwater depletion: An analysis of the GRACE signal in Morocco. *J. Hydrol. Reg. Stud.* **2022**, *42*, 101177. [CrossRef]
19. Boudhar, A.; Baba, W.M.; Marchane, A.; Ouatiki, H.; Bouamri, H.; Hanich, L.; Chehbouni, A. Water Resources Monitoring Over the Atlas Mountains in Morocco Using Satellite Observations and Reanalysis Data. In *Remote Sensing of African Mountains*; Springer: Cham, Switzerland, 2022; pp. 157–170. [CrossRef]
20. Chadli, K. Estimation of Soil Loss Using RUSLE Model for Sebou Catchment (Morocco). *Model. Earth Syst. Environ.* **2016**, *2*, 1–10. [CrossRef]
21. Serpa, D.; Nunes, J.P.; Santos, J.; Sampaio, E.; Jacinto, R.; Veiga, S.; Lima, J.C.; Moreira, M.; Corte-Real, J.; Keizer, J.J.; et al. Impacts of climate and land use changes on the hydrological and erosion processes of two contrasting Mediterranean catchments. *Sci. Total Environ.* **2015**, *538*, 64–77. [CrossRef]

22. Jacob, D.; Petersen, J.; Eggert, B.; Alias, A.; Christensen, O.B.; Bouwer, L.M.; Braun, A.; Colette, A.; Déqué, M.; Georgievski, G.; et al. EURO-CORDEX: New high-resolution climate change projections for European impact research. *Reg. Environ. Chang.* **2014**, *14*, 563–578. [CrossRef]
23. Dee, D.P.; Uppala, S.M.; Simmons, A.J.; Berrisford, P.; Poli, P.; Kobayashi, S.; Andrae, U.; Balmaseda, M.A.; Balsamo, G.; Bauer, P.; et al. The ERA-Interim reanalysis: Configuration and performance of the data assimilation system. *Q. J. R. Meteorol. Soc.* **2011**, *137*, 553–597. [CrossRef]
24. Dobler, C.; Hagemann, S.; Wilby, R.L.; Stötter, J. Quantifying different sources of uncertainty in hydrological projections in an Alpine catchment. *Hydrol. Earth Syst. Sci.* **2012**, *16*, 4343–4360. [CrossRef]
25. Minville, M.; Brissette, F.; Leconte, R. Uncertainty of the impact of climate change on the hydrology of a nordic catchment. *J. Hydrol.* **2008**, *358*, 70–83. [CrossRef]
26. Marchane, A.; Tramblay, Y.; Hanich, L.; Ruelland, D.; Jarlan, L. Climate change impacts on surface water resources in the Rheraya catchment (High Atlas, Morocco). *Hydrol. Sci. J.* **2017**, *62*, 979–995. [CrossRef]
27. Teutschbein, C.; Seibert, J. Bias correction of regional climate model simulations for hydrological climate-change impact studies: Review and evaluation of different methods. *J. Hydrol.* **2012**, *456*, 12–29. [CrossRef]
28. Wilby, R.L.; Harris, I. A framework for assessing uncertainties in climate change impacts: Low-flow scenarios for the River Thames, UK. *Water Resour. Res.* **2006**, *42*. [CrossRef]
29. Gavrilovic, S. A method for estimating the average annual quantity of sediments according to the potency of erosion. *Bull. Fac. For.* **1962**, *26*, 151–168.
30. Gavrilovic, S. Modern ways of calculating the torrential sediment and erosion mapping. In *Erosion, Torrents and Alluvial Deposits*; Yugoslav Committee for International Hydrological Decade: Belgrade, Serbia, 1970; pp. 85–100.
31. Gavrilovic, S. *Engineering of Torrential Flows and Erosion*; Izgradnja: Belgrade, Serbia, 1972; 272p.
32. Chaaouan, J.; Faleh, A.; Sadiki, A.; Mesrar, H. Télédétection, SIG et modélisation de l'érosion hydrique dans le bassin versant de l'oued Amzaz, Rif Central. *Rev. Française De Photogrammétrie Et De Télédétection* **2013**, *203*, 19–25. [CrossRef]
33. Zorgan, G. The use of an Empirical Method (Erosion Potential Method) for Calculating Sediment Production and Transportation in Unstudied or Torrential Stream. In *Proceeding of International Conference on River Regimen*; Hydraulics Research Limited: Wallingford, Oxon, UK, 1988.
34. El Khalki, E.M.; Tramblay, Y.; Hanich, L.; Marchane, A.; Boudhar, A.; Hakkani, B. Climate change impacts on surface water resources in the Oued El Abid basin, Morocco. *Hydrol. Sci. J.* **2021**, *66*, 2132–2145. [CrossRef]
35. Tuel, A.; Kang, S.; Eltahir, E.A.B. Understanding climate change over the southwestern Mediterranean using high-resolution simulations. *Clim. Dyn.* **2021**, *56*, 985–1001. [CrossRef]
36. Gallardo, C.; Arribas, A.; Prego, J.A.; Gaertner, M.A.; De Castro, M. Multi-year simulations using a regional-climate model over the Iberian Peninsula: Current climate and doubled CO_2 scenario. *Q. J. R. Meteorol. Soc.* **2001**, *127*, 1659–1681. [CrossRef]
37. Bergant, K.; Belda, M.; Halenka, T. Systematic errors in the simulation of European climate (1961–2000) with RegCM3 driven by NCEP/NCAR reanalysis. *Int. J. Climatol.* **2007**, *27*, 455–472. [CrossRef]
38. Berteni, F.; Grossi, G. Water soil erosion evaluation in a small alpine catchment located in northern Italy: Potential effects of climate change. *Geosciences* **2020**, *10*, 386. [CrossRef]
39. Stefanidis, S.; Stathis, D. Effect of climate change on soil erosion in a mountainous Mediterranean catchment (Central Pindus, Greece). *Water* **2018**, *10*, 1469. [CrossRef]
40. Ennaji, N.; Ouakhir, H.; Halouan, S.; Abahrour, M. Assessment of soil erosion rate using the EPM model: Case of Ouaoumana basin, Middle Atlas, Morocco. In *IOP Conference Series: Earth and Environmental Science*; IOP Publishing: Bristol, UK, 2022; Volume 1090, p. 012004. [CrossRef]
41. Marouane, L.; Lahcen, B.; Valérie, M. Assessment and mapping of water erosion by the integration of the Gavrilovic "EPM" model in the Inaouene watershed, Morocco. In *E3S Web of Conferences*; EDP Sciences: Les Ulis, France, 2021; Volume 314, p. 03009.
42. Ouallali, A.; Aassoumi, H.; Moukhchane, M.; Moumou, A.; Houssni, M.; Spalevic, V.; Keesstra, S. Sediment mobilization study on Cretaceous, Tertiary and Quaternary lithological formations of an external Rif catchment, Morocco. *Hydrol. Sci. J.* **2020**, *65*, 1568–1582. [CrossRef]
43. El Jazouli, A.; Barakat, A.; Khellouk, R.; Rais, J.; El Baghdadi, M. Remote sensing and GIS techniques for prediction of land use land cover change effects on soil erosion in the high basin of the Oum Er Rbia River (Morocco). *Remote Sens. Appl. Soc. Environ.* **2019**, *13*, 361–374. [CrossRef]
44. Acharki, S.; El Qorchi, F.; Arjdal, Y.; Amharref, M.; Bernoussi, A.S.; Aissa, H.B. Soil erosion assessment in Northwestern Morocco. *Remote Sens. Appl. Soc. Environ.* **2022**, *25*, 100663. [CrossRef]
45. Berteni, F.; Barontini, S.; Grossi, G. Evaluating soil erosion by water in a small alpine catchment in Northern Italy: Comparison of empirical models. *Acta Geochim.* **2021**, *40*, 507–524. [CrossRef]